Matrix Biology 140 (2025) 16–26

Contents lists available at ScienceDirect

Matrix Biology

journal homepage: www.elsevier.com/locate/matbio

A complex relationship between the architecture of the basement membrane, its mechanical properties, and its ability to shape the Drosophila egg

Mitchell T. Anderson [a,b], Sally Horne-Badovinac [a,b,*]

[a] Department of Molecular Genetics and Cell Biology, The University of Chicago, 920 East 58th Street, Chicago, IL 60637, USA
[b] Committee on Development, Regeneration, and Stem Cell Biology, The University of Chicago, 920 East 58th Street, Chicago, IL 60637, USA

ARTICLE INFO

Keywords:
Basement membrane
Tissue elongation
Extracellular matrix
Morphogenesis
Architecture
Mechanics
Drosophila
Egg chamber

ABSTRACT

Basement membranes (BMs) are planar extracellular matrices that line the basal surfaces of epithelia and are essential components of most organs. During development, BMs can also play instructive roles in shaping the tissues to which they belong, but how they do so is incompletely understood. The *Drosophila* egg chamber has become a premier system to study this aspect of BM biology due to the ostensible simplicity of the BM's role in morphogenesis. The prevailing model posits that the egg chamber's outer layer of epithelial cells creates a symmetric stiffness gradient in the surrounding BM that preferentially channels egg chamber growth along one axis to create the elongated shape of the egg. There is evidence that the stiffening of the BM depends, in part, on a polarized array of fibrils that form within the BM network, and yet the exact role the BM fibrils play in egg chamber elongation has remained unclear. Here, we use genetic conditions that abrogate fibril formation to different extents to probe the relationship between the BM's fibril content, its mechanical properties, and the shape of the egg. The results of these experiments are consistent with a model in which BM fibrils influence egg shape by directly augmenting the mechanical properties of the BM. However, we then examine a final genetic condition that does not fit this simple narrative. We propose that the role of the BM in conferring final egg shape is more complicated than previously thought and that some approaches used to study this role should be re-evaluated for their efficacy.

Introduction

Basement membranes (BMs) are sheet-like extracellular matrices (ECMs) that line the basal surfaces of epithelia and are essential components of most organs [1,2]. They are formed from independent networks of type IV collagen and laminin that are linked together by nidogen and heparin sulfate proteoglycans like perlecan. Although all BMs are assembled from this same set of core proteins, they can also show remarkable diversity in other aspects of their molecular composition, their architecture, and their mechanical properties. This diversity allows BMs to perform a variety of functions that are tailored to the physiological needs of the tissues to which they belong [3–5]. It is increasingly appreciated that BMs also play key roles in tissue morphogenesis [6–11], but how BMs perform this function is incompletely understood.

The *Drosophila* egg chamber provides a powerful system to define how a BM influences tissue elongation [12,13]. An egg chamber is an ovarian follicle composed of a germ cell cyst with one oocyte and fifteen nurse cells, surrounded by a somatic epithelium called the follicle cells. The entire organ is encased in a BM (Fig. 1A). Each egg chamber lengthens along its anterior-posterior (AP) axis as it grows, progressing through 14 developmental stages before becoming an ellipsoidal egg. This morphogenesis depends on mechanical patterning of the BM, which is secreted and assembled by the follicle cells [14–16]. During the first 8 stages of oogenesis, the follicle cells create a stiffness gradient within the BM, in which stiffness is highest in the center and lowest at the anterior and posterior poles [17,18]. This stiffness gradient is then thought to allow the BM to provide anisotropic resistance to tissue growth and thereby bias that growth along the AP axis to lengthen the tissue (Fig. 1B).

How the stiffness gradient forms in the BM is unknown, but it is typically associated with a rotational collective migration of the follicle

* Corresponding author.
E-mail address: shorne@uchicago.edu (S. Horne-Badovinac).

https://doi.org/10.1016/j.matbio.2025.06.001
Received 31 January 2025; Received in revised form 23 May 2025; Accepted 12 June 2025
Available online 13 June 2025

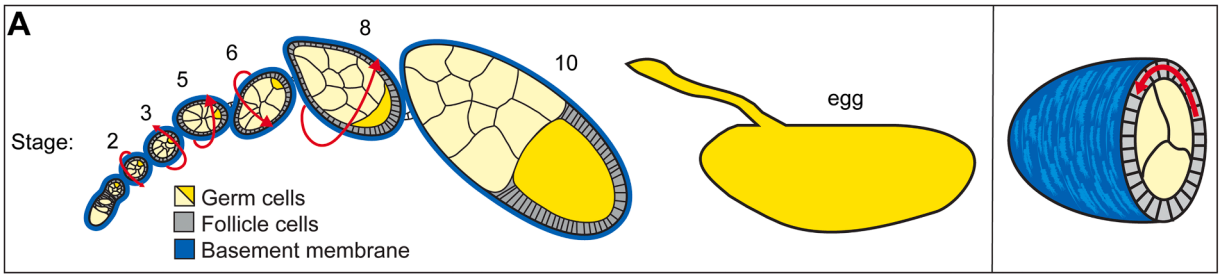

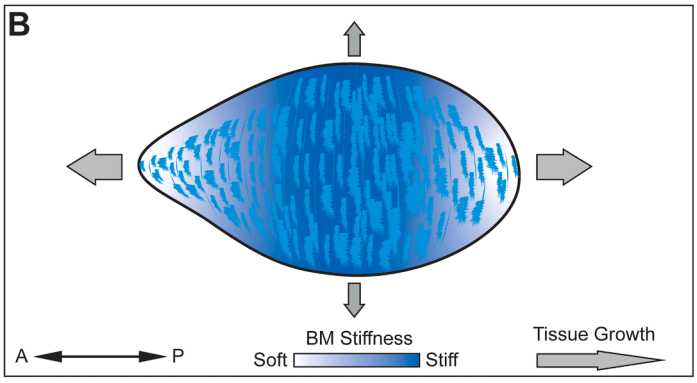

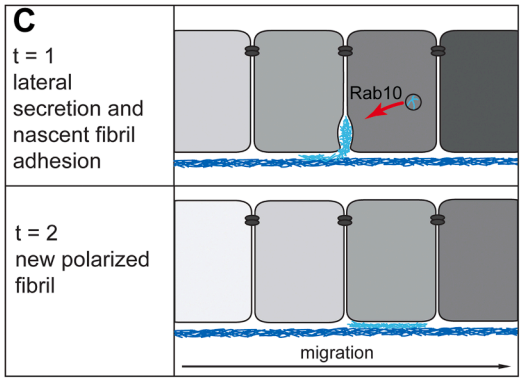

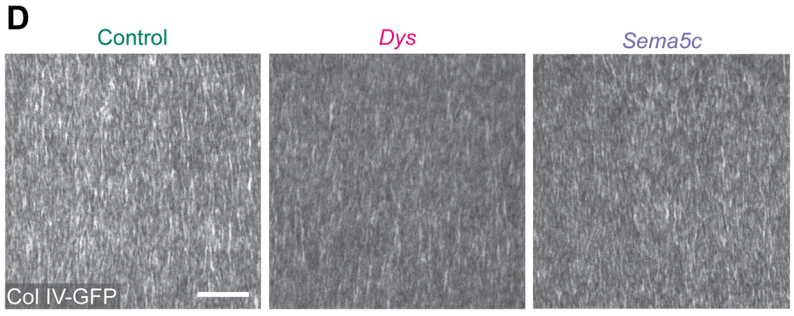

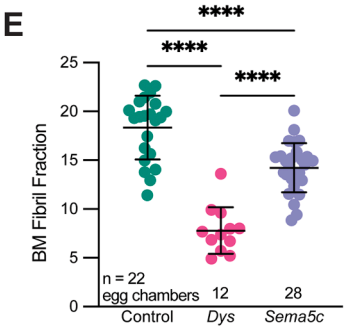

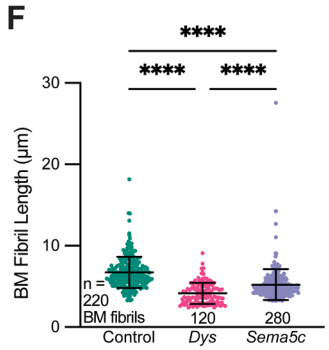

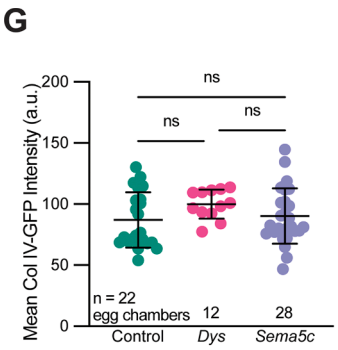

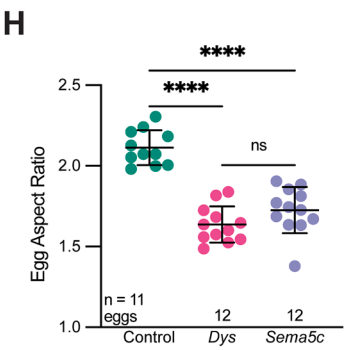

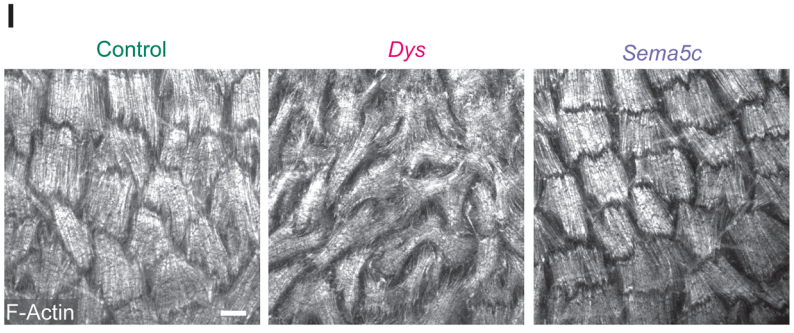

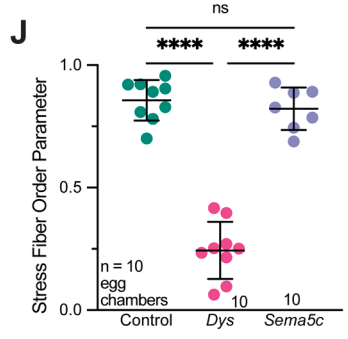

(caption on next page)

Fig. 1. Introduction to the BM's role in egg chamber elongation and the *Sema5c* BM defect. (A) Left, Illustration of a sagittal section of a developmental array of egg chambers. Arrows indicate stages at which follicle cells undergo rotational migration. Right, illustration of a transverse section through an egg chamber. BM fibrils are in light blue and the underlying matrix is in dark blue. Arrow indicates follicle cell migration. (B) Illustration of the stiffness gradient in the BM and its hypothesized role in directing egg chamber growth along the AP axis. BM fibrils are in light blue. (C) Illustration of how migration and BM protein secretion synergize to form polarized BM fibrils. (D) Images showing BM architecture for control, *Dys*, and *Sema5c* egg chambers at stage 8. (E, F) Quantifications of BM fibril fraction and length. Loss of either *Dys* or *Sema5c* both reduces and shortens BM fibrils. (G) Quantification of mean Col IV-GFP intensity. Loss of *Dys* or *Sema5c* does not alter the amount of Col IV-GFP in the BM. The same egg chambers are used in (E-G). (H) Quantification of egg aspect ratios. Loss of either *Dys* or *Sema5c* results in similar rounding of the egg. (I) Images of global stress fiber alignment in control, *Dys*, and *Sema5c* egg chambers at stage 13. (J) Quantification of stress fiber order parameter. Loss of *Dys* causes stress fiber misalignment, whereas loss of *Sema5c* does not. (E-H, J) Data represent mean ± SD. (E-G) Welch's ANOVA with Dunnett's T3 multiple comparisons test; ns, $p > 0.05$; ****$p < 0.0001$. (H and J) Ordinary one-way ANOVA with Tukey's multiple comparisons test; ns, $p > 0.05$; ****$p < 0.0001$. (D, I) Scale bars, 10 μm.

cells in which the BM serves as the stationary substrate on which the cells crawl (Fig. 1A) [19,20]. Between stages 5 and 8 of oogenesis, this motion synergizes with a Rab10-dependent trafficking pathway that targets new BM protein secretion in between the follicle cells to create a polarized array of fibrils within the matrix that is oriented perpendicular to the axis of elongation (Fig. 1A–C) [15,19,21–23]. The fibrils are assembled from at least three BM proteins (Collagen IV, Laminin, and Perlecan) [21], which suggests that these structures may simply be a linear form of the BM network. The fibrils increase the stiffness of the BM [17,24,25], and artificially increasing the BM's fibril content by over-activating the Rab10 pathway can hyper-elongate the egg [21]. Together, these findings suggest that fibrils directly contribute to the mechanical patterning of the BM that shapes the egg. However, studies of the BM receptor Dystroglycan and its cytoplasmic adaptor Dystrophin (Dys) suggested an alternate model in which BM fibrils shape the egg by serving as a template for the global alignment of contractile stress fibers across the epithelium during stages 12–14 [26]. Whether stress fibers promote egg chamber elongation during these final stages of oogenesis is unclear; complex genetic experiments involving *Dys* suggest that they do [26], and yet acute removal of the F-actin cytoskeleton with latrunculin at stage 12 has no effect on egg chamber shape [19]. Thus, whether BM fibrils play a stress fiber-independent role in shaping the egg by directly augmenting BM mechanics remains an open question.

In this study, we use genetic conditions that abrogate fibril formation to different extents to probe the relationship between the BM's fibril content, its mechanical properties, and the shape of the egg. Notably, we identify a condition in which BM fibrils are reduced without an accompanying defect in late-stage stress fiber alignment and then use this condition to make a strong case that BM fibrils help to shape the egg by directly augmenting the mechanical properties of the BM. However, we then show a final set of results that do not fit this simple narrative. We propose that the role of the BM in conferring final egg shape is more complicated than previously thought and that some approaches used to study this role should be re-evaluated for their efficacy

Results

To gain deeper insight into the role of the BM in shaping the egg, we started with a genetic condition in which BM fibrils are reduced. Previous work from our lab had shown that the transmembrane semaphorin, Semaphorin 5c (Sema5c), functions as part of a planar signaling system that promotes follicle cell migration, and that loss of Sema5c impairs this motion [27,28]. This is consistent with the well-established role of semaphorin family proteins in guiding the migratory behaviors of neurons and other cells types [29–31]. During these studies, we noticed that *Sema5c* epithelia also have an architectural defect in their BMs that is likely secondary to the defect in follicle cell migration. Because the architectural defect in the BMs of *Sema5c* egg chambers looks remarkably like that caused by loss of Dys [26], we quantitatively compared the two phenotypes. The most abundant protein in the basement membrane is Collagen IV, which is a trimer composed of two α1 chains and one α2 chain. We visualized the BM using an endogenous GFP tag on the α2 chain, called Viking in *Drosophila* (Col IV-GFP) [32], and analyzed its architecture by determining the fraction of BM GFP fluorescence that is contained in fibrils (fibril fraction, Fig. S1A) [21]. We found that BM fibrils are both reduced and shorter in epithelia lacking either Sema5c or Dys, and that the two conditions cause similar rounding of the egg (Fig. 1D–H). However, unlike the epithelia lacking Dys that have mis-aligned stress fibers at stage 13, the stress fibers are properly aligned in epithelia lacking Sema5c at this stage (Fig. 1I, J). We note that the reduction in BM fibrils is milder in *Sema5c* epithelia than in *Dys* epithelia which could account for the difference in stress fiber alignment. Altogether, these results suggested that *Sema5c* egg chambers might provide a loss-of-function condition in which to study the stress fiber-independent role of BM fibrils in shaping the egg.

We hypothesized that *Sema5c* eggs are rounder than controls because the developing egg chambers are surrounded by weakened BMs that are unable to properly channel tissue growth along the AP axis. Given that Col IV is thought to provide tensile strength to BMs, we first asked if we could dominantly enhance the *Sema5c* egg shape defect using the *BSC172* deficiency, which is a small chromosomal deletion that removes the genes encoding the α1 and α2 chains of Col IV and very few others. When this deficiency is present in one copy in otherwise wild-type females, eggs are properly elongated. By contrast, introducing the deficiency into *Sema5c* females made their eggs rounder (Fig. 2A). Evidence that Col IV levels are, in fact, reduced by the deficiency comes from the observation that Perlecan levels (Trol in *Drosophila,* Trol-GFP) are also reduced in this background (Fig. S1B, C), as the incorporation of Perlecan into the follicular BM strongly depends on Col IV [18,19,33]. Notably, the deficiency only minorly enhances the follicle cell migration defect associated with loss of Sema5c (Fig. 2B), suggesting that the enhancement of the egg shape defect is specific to the BM.

We then asked if it is the loss of BM fibrils, specifically, that causes the defect in egg elongation. We overexpressed Rab10 in *Sema5c* epithelia in a way that restored BM fibrils to wild-type levels and lengths and found that this fully suppressed the egg shape defect (Fig. 2C–G). This manipulation also caused a slight decrease in the mean Col IV-GFP intensity in the BM, which we attribute to small amounts of Col IV-GFP becoming aberrantly localized below the adherens junctions (Fig. 2F and S1D). Thus, restoring the fibrillar organization of the BM can even compensate for slight reductions in Col IV levels, which would normally be predicted to enhance the egg shape defect. Our ability both to enhance and to suppress the round egg phenotype in *Sema5c* females simply by manipulating the BM strongly suggests that a weakened BM is, in fact, responsible for this phenotype. Moreover, the Rab10 experiment supports the idea that the loss of fibrils could cause the BM to be weakened.

The round egg phenotype caused by loss of Sema5c is milder than that seen in some other genetic conditions that disrupt follicle cell migration (Fig. 3A). For example, loss of the atypical cadherin Fat2 completely blocks migration, and the egg is nearly spherical [34–36]. By contrast, loss of Sema5c delays the onset of migration and slows it thereafter, and the egg is only mildly round [27]. Epithelia lacking Fat2 have extreme defects in their BM architecture in which the BM proteins that would have formed fibrils instead accumulate in rings around the basal surface of each cell because they are unable to attain their polarized orientation in the absence of tissue movement (Fig. 3B) [21]. This architectural difference correlates with a profound defect in BM

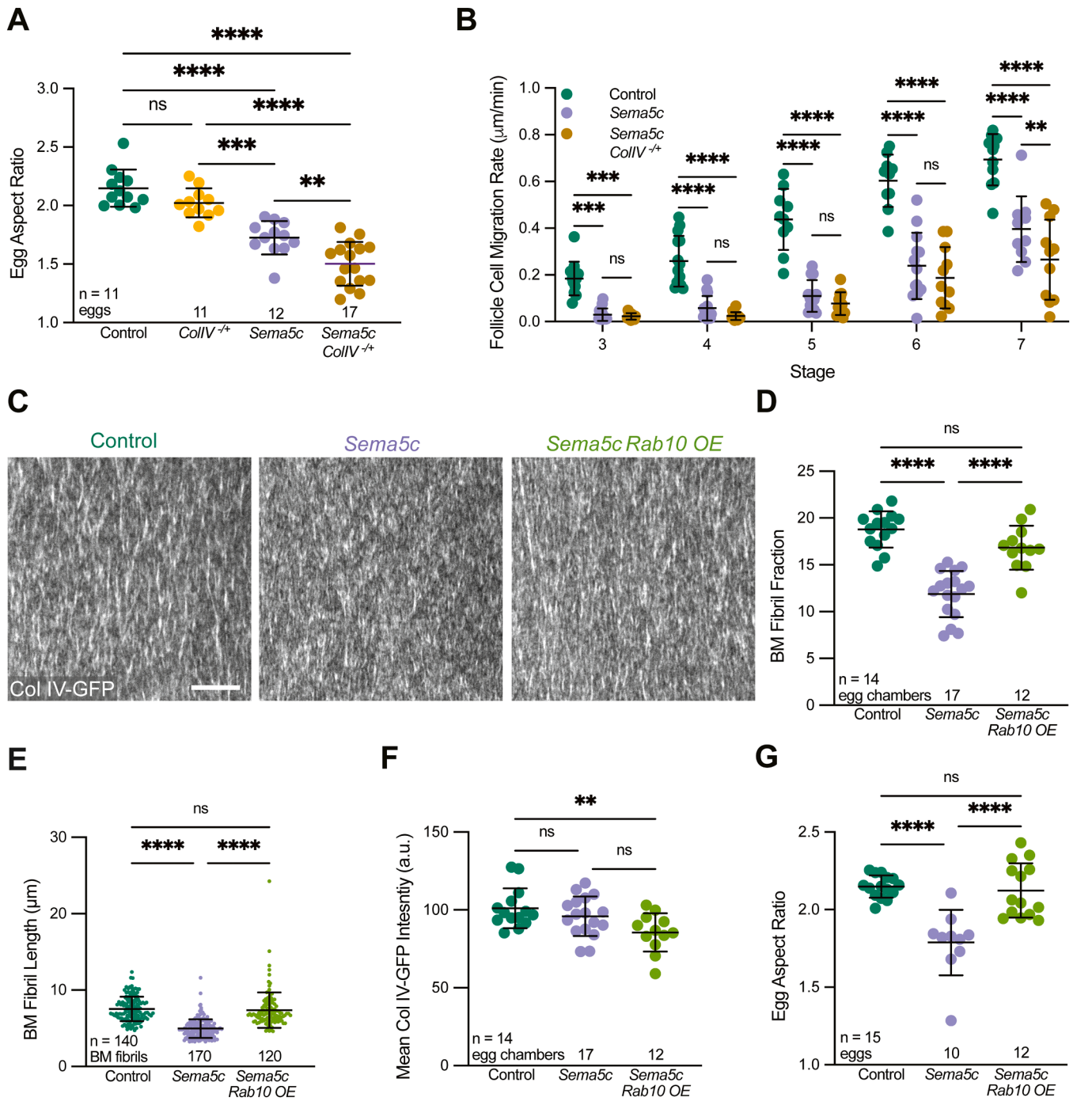

Fig. 2. BM-specific manipulations can enhance or suppress the *Sema5c* egg shape defect. (A) Quantification of egg aspect ratios. Removing one copy of the genes encoding the α1 and α2 chains of Col IV with a chromosomal deficiency enhances the *Sema5c* egg shape defect. Data for control and *Sema5c* are the same as in Fig. 1H. (B) Quantification of follicle cell migration rates. Removing one copy of the genes encoding Col IV only minorly enhances the *Sema5c* migration defect. See **Table S4** for sample sizes. (C) Images showing BM architecture in control, *Sema5c*, and *Sema5c Rab10 OE* egg chambers at stage 8. (D, E) Quantification of the BM fibril fraction and fibril lengths. Overexpressing *Rab10* restores the fibrils in *Sema5c* BMs to wild-type levels and lengths. (F) Quantification of mean Col IV-GFP intensity. Overexpressing *Rab10* slightly decreases the amount of Col IV-GFP in *Sema5c* BMs. The same egg chambers are used in (D-F). (G) Quantification of egg aspect ratios. Overexpressing *Rab10* suppresses the *Sema5c* egg shape defect. (A, B, D-G) Data represent mean ± SD. (A, D-G) Ordinary one-way ANOVA with Tukey's multiple comparisons test; ns, $p > 0.05$; $^{**}p < 0.01$; $^{***}p < 0.001$; $^{****}p < 0.0001$. (B) Ordinary two-way ANOVA with Tukey's multiple comparisons test; ns, $p > 0.05$; $^{**}p < 0.01$; $^{***}p < 0.001$; $^{****}p < 0.0001$. (C) Scale bar, 10 µm.

mechanics [17,24]. If our central hypothesis is correct, the mild rounding of *Sema5c* eggs should correlate with milder defects in BM mechanics than those caused by loss of Fat2, so we next compared these two conditions.

We initially determined when in development the elongation defect first becomes apparent in *Sema5c* egg chambers by measuring their aspect ratios over time. It was previously known that wild-type egg chambers elongate steadily from stages 4–14 and that *fat2* egg chambers follow the same trajectory until stage 7 before becoming rounder than controls [37,38]. We found that *Sema5c* egg chambers properly elongate for a longer period than *fat2* egg chambers, only becoming rounder than controls at stage 12 (Fig. 3C).

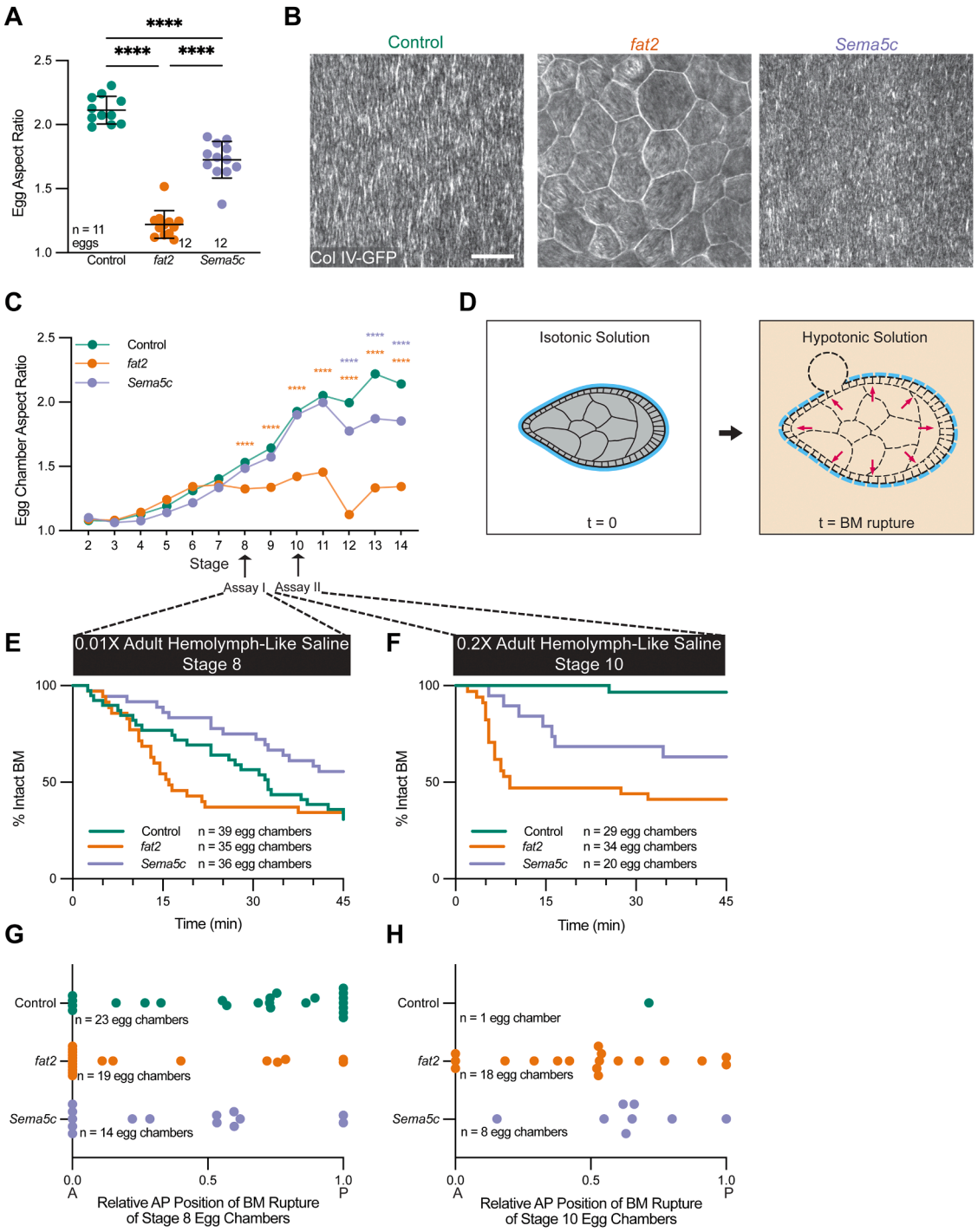

Fig. 3. A BM mechanical defect is detectable just before the elongation defect in *Sema5c* egg chambers. (A) Quantification of egg aspect ratios. *Sema5c* eggs are less round than *fat2* eggs. Data for control and *Sema5c* are same as in Fig. 1H. Data represent mean ± SD. Ordinary one-way ANOVA with Tukey's multiple comparisons test; ****$p < 0.0001$. (B) Images showing BM architecture for control, *fat2*, and *Sema5c* egg chambers at stage 8. (C) Quantification of egg chamber aspect ratio over development. *Sema5c* egg chambers become rounder than controls later than *fat2* egg chambers. Data represent mean. Ordinary two-way ANOVA with Tukey's multiple comparisons test; ****$p < 0.0001$. Orange stars compare *fat2* egg chambers to controls. Purple stars compare *Sema5c* egg chambers to controls. See **Table S5** for sample sizes and additional p values. (D) Illustration of an osmotic swelling assay. Egg chambers are placed into a hypotonic solution, causing them to swell and their BMs to rupture. BM is in light blue. (E) Kaplan-Meier curve of a swelling assay on control, *fat2*, and *Sema5c* egg chambers at stage 8. The BMs of Sema5c egg chambers are slightly more resistant to rupturing than controls. (F) Kaplan-Meier curve of a swelling assay on control, *fat2*, and *Sema5c* egg chambers at stage 10. The BMs of *Sema5c* egg chambers rupture at a rate that is intermediate between those of control and *fat2* egg chambers. (G) Graph of the AP position of BM rupture in control, *fat2*, and *Sema5c* egg chambers at stage 8. Only egg chambers that ruptured in (E) are plotted here. (H) Graph of the AP position of BM rupture in control, *fat2*, and *Sema5c* egg chambers at stage 10. Only egg chambers that ruptured in (F) are plotted here. (B) Scale bar, 10 μm.

We then asked if the difference in elongation dynamics between *Sema5c* and *fat2* egg chambers could be explained by differences in the mechanical properties of their BMs. To this end, we used an osmotic swelling assay, in which egg chambers are placed into a hypotonic solution and rapidly increase in size as the cells take on water [17,39]. This imposes stresses on the surrounding BM that can cause it to rupture (Fig. 3D). Defects in the mechanical properties of the BM have been linked to changes in the rate, frequency, and position of this rupture event [17,40]. We first performed this assay at stage 8. This is standard for the field [17,18,40,41], as this is the stage when fibril formation and Col IV levels have both peaked [19,21,33], as Col IV synthesis and the rotational migration that is required for BM fibrils to form both stop after this stage [19,42]. Consistent with prior results, the BMs of *fat2* egg chambers ruptured more quickly than those of wild-type egg chambers (Fig. 3E) [17]. We predicted that the BMs of *Sema5c* egg chambers would rupture at a rate that is intermediate between that of *fat2* and wild-type egg chambers but instead found that the BMs of *Sema5c* egg chambers ruptured slightly more slowly than the wild-type condition at this stage (Fig. 3E).

Given that *Sema5c* egg chambers do not become rounder than controls until stage 12, we reasoned that a mechanical defect in their BMs might not be observable until later in development, so we adapted the swelling assay for use on egg chambers at stage 10. It quickly became apparent that the BMs of stage 10 egg chambers rupture more quickly than at stage 8, which necessitated the use of a milder hypotonic solution that provided a good dynamic range for the three genotypes of interest (Fig. S2A-C). Notably, performing the swelling assay at stage 10 revealed the behavior we predicted for the BMs of *Sema5c* egg chambers

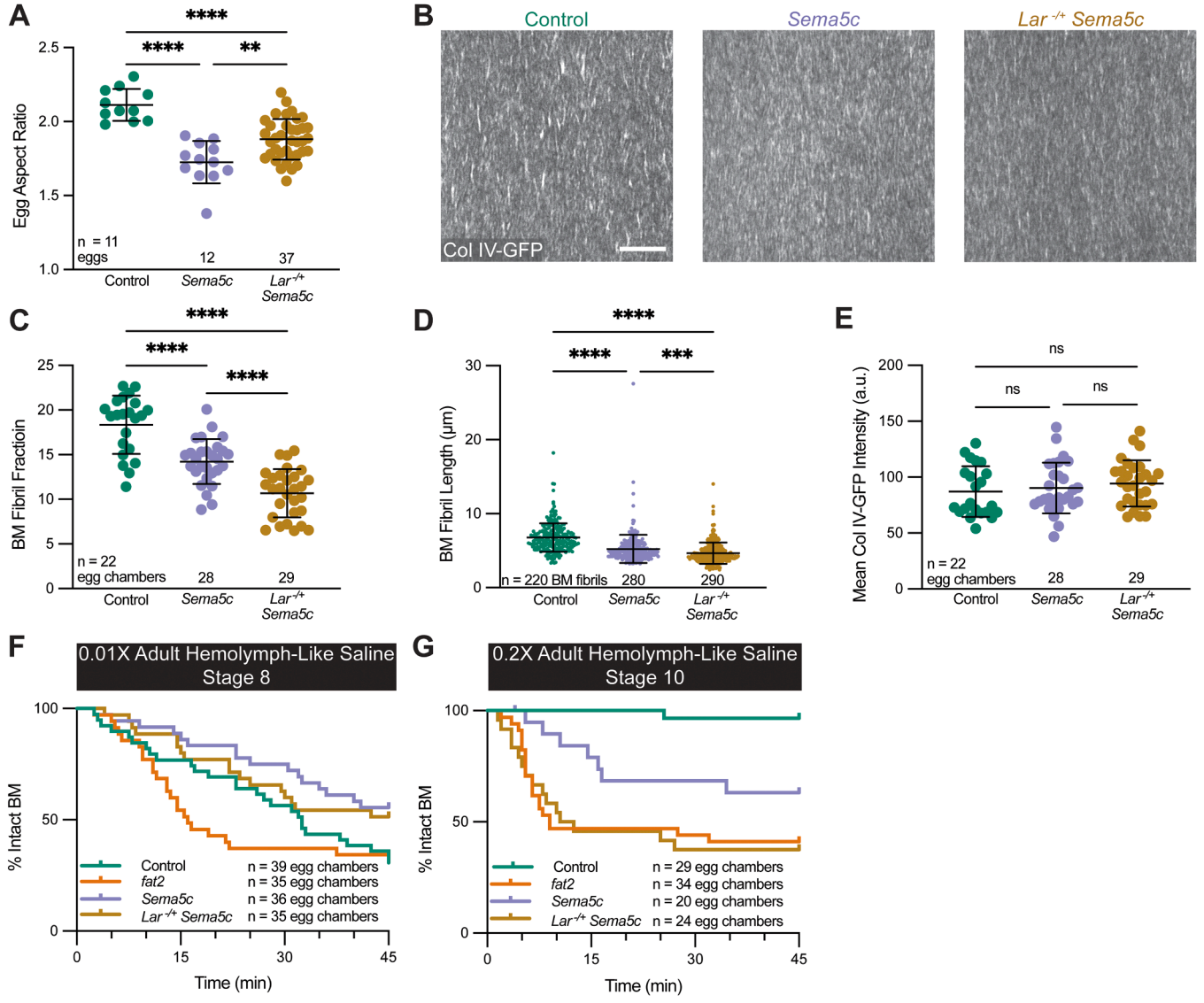

Fig. 4. Removing one copy of *Lar* suppresses the *Sema5c* egg shape defect without restoring proper BM architecture or mechanical properties. (A) Graph of egg aspect ratios. Removing one copy of *Lar* suppresses the *Sema5c* egg shape defect. Data for control and *Sema5c* are same as in Fig. 1H. (B) Images of BM architecture in control, *Sema5c*, and $Lar^{-/+}$ *Sema5c* egg chambers at stage 8. (C, D) Quantification of BM fibril fraction and length. Removing one copy of *Lar* enhances the loss of fibrils normally seen in *Sema5c* BMs and makes them even shorter. Data for control and *Sema5c* are the same as in Fig. 1E, F. (E) Quantification of mean Col IV-GFP intensity. Loss of *Sema5c* by itself or while also removing one copy of *Lar* does not affect the amount of Col IV-GFP in the BM. Data for control and *Sema5c* are the same as in Fig. 1G. The same egg chambers are used in (C-E). (F) Kaplan-Meier curve of a swelling assay on control, *fat2, Sema5c*, and $Lar^{-/+}$ *Sema5c* egg chambers at stage 8. Removing one copy of *Lar* in *Sema5c* egg chambers has little effect at this stage. Data for the first three conditions are the same as in Fig. 3E. (G) Kaplan-Meier curve of a swelling assay on control, *fat2, Sema5c*, and $Lar^{-/+}$ *Sema5c* egg chambers at stage 10. Removing one copy of *Lar* in *Sema5c* egg chambers increases the rate and frequency of BM rupture. Data for the first three conditions are the same as in Fig. 3F. (A, C-E) Data represent mean ± SD. Ordinary one-way ANOVA with Tukey's multiple comparisons test; ns, $p > 0.05$; $^{**}p < 0.01$; $^{***}p < 0.001$; $^{****}p < 0.0001$. (B) Scale bar, 10 µm.

- they ruptured at a rate intermediate between those of control and *fat2* egg chambers (Fig. 3F). There was no obvious difference in the distribution of rupture position between the three conditions at either stage (Fig. 3G, H). The observation that the defect in BM mechanics does not become apparent in *Sema5c* egg chambers until shortly before the elongation defect supports a causal relationship between the two phenotypes. Our results further suggest that the difference in egg shape between the *Sema5c* and *fat2* conditions could be due to differences in the mechanical properties of their BMs.

Up to this point, all our results had supported our central hypothesis: the eggs produced by *Sema5c* females have a rounded morphology due to the developing egg chambers having fewer BM fibrils and mechanically weakened BMs. However, we then performed a final set of experiments that challenged this idea. We previously identified a genetic condition that dominantly suppresses the egg shape defect in *Sema5c* females - removal of one copy of the gene encoding the receptor tyrosine phosphatase Lar (*Lar*$^{-/+}$ *Sema5c*), which is a protein that works with Sema5c to promote follicle cell migration [27]. We have repeated this result here (Fig. 4A). If our hypothesis is correct, this condition should also restore BM fibrils and/or BM mechanics back to wild-type levels. Instead, we observed the opposite result. Removing one copy of *Lar* further decreases fibril content and length in *Sema5c* BMs (Fig. 4B–D), despite Col IV-GFP and Trol-GFP levels being equivalent between the two conditions (Fig. 4B, E and S3A, B). The BMs of *Lar*$^{-/+}$ *Sema5c* egg chambers also rupture more quickly in osmotic swelling assays at stage 10 than those lacking Sema5c alone (Fig. 4F, G). Thus, the BM appears to be even further weakened in the *Lar*$^{-/+}$ *Sema5c* egg chambers, at least in terms of its ability to resist rupture following acute swelling.

Given these unexpected results, we considered factors that could conceivably compensate for the weakened BMs of *Lar*$^{-/+}$ *Sema5c* egg chambers such that normally elongated eggs are still produced. First, we asked if late-stage stress fibers might provide this compensation. Prior work has shown that acute disruption of the actin cytoskeleton with latrunculin in wild-type egg chambers at stages 12–13 has no effect on egg chamber shape [19]. We found that the stress fibers in *Lar*$^{-/+}$ *Sema5c* egg chambers look equivalent to controls at stage 13 (Fig. 5A, B), and that treating these egg chambers with latrunculin similarly had no effect on their shape (Fig. 5C). We note that a small amount of F-actin is still present at the basal surfaces of some follicle cells after the latrunculin treatment (Fig. S3C). However, the F-actin is missing from enough cells that a circumferential contractile network is no longer formed. Thus, stress fibers seem unlikely to compensate for a weakened BM in *Lar*$^{-/+}$ *Sema5c* egg chambers.

We then considered a potential role for the muscle sheath that surrounds the developing egg chambers in the ovary, as defects in the contractile activity of this tissue can affect the aspect ratio of the egg [43]. However, changes in muscle activity also reduce the volume of the egg [43]. Because the volume of the eggs is conserved in *Lar*$^{-/+}$ *Sema5c* females (Fig. 5D), this seems unlikely as well.

Finally, we used collagenase to digest away the BM from *Lar*$^{-/+}$ *Sema5c* egg chambers at stage 12–13 and found that this caused the egg chambers to become rounder (Fig. 5E and S3D), as has been previously described for wild-type egg chambers at this stage [19]. Altogether, these results suggest that the BM continues to be a key factor that determines the shape of *Lar*$^{-/+}$ *Sema5c* egg chambers, despite its reduced fibril content and reduced ability to resist rupture following acute tissue swelling. These unexpected results are discussed in detail below.

Discussion

The idea that BMs can play an instructive role in morphogenesis has become well accepted in recent years, with this phenomenon now being

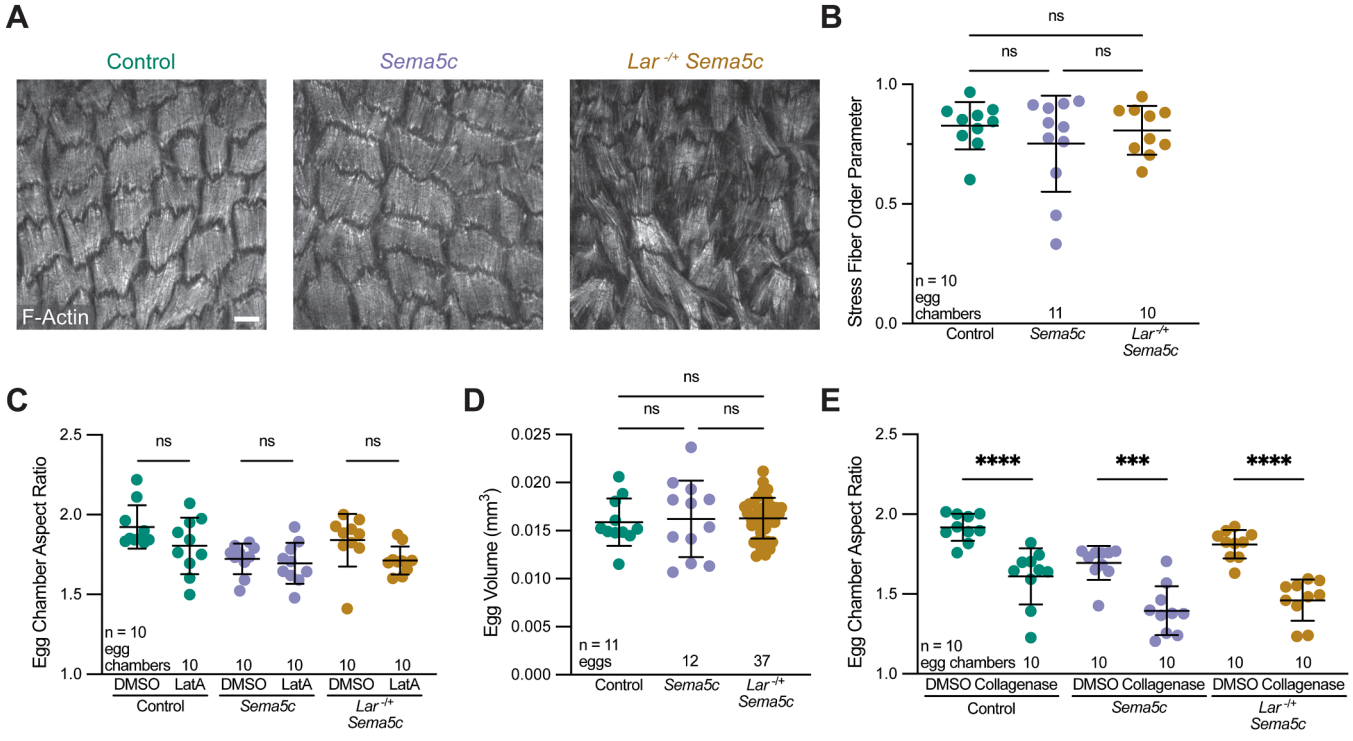

Fig. 5. The BM is required to maintain the shape of *Lar*$^{-/+}$ *Sema5c* egg chambers. (A) Images of global stress fiber alignment in control, *Sema5c*, and *Lar*$^{-/+}$ *Sema5c* egg chambers at stage 13. (B) Quantification of stress fiber order parameter. Loss of *Sema5c* alone or while also removing one copy of *Lar* has no effect on global stress fiber alignment. (C) Graph of egg chamber aspect ratio following latrunculin A (LatA) or DMSO vehicle treatment at stage 12 or 13. Treatment with latrunculin does not cause rounding of egg chambers. (D) Graph of egg volume. Egg volume is the same for control, *Sema5c*, and *Lar*$^{-/+}$ *Sema5c* eggs. Eggs used for this measurement are the same as in Fig. 4A. (E) Graph of egg chamber aspect ratio following collagenase or DMSO vehicle treatment at stage 12 or 13. Treatment with collagenase causes egg chambers to become rounder. (B-E) Data represent mean ± SD. (B, D) Ordinary one-way ANOVA with Tukey's multiple comparisons test; ns, $p > 0.05$. (C, E) Unpaired t-test with Welch's correction; ns, $p > 0.05$; ***$p < 0.001$; ****$p < 0.0001$. (A) Scale bar, 10 μm.

documented in a wide range of tissues and organisms [6–11]. Studies performed in the egg chamber were foundational to this understanding, and the egg chamber continues to be the experimental system where we know the most about how polarized secretion [21,22,44], migration-assisted assembly [19,21], and enzymatic remodeling [40,41,45–47] work together to create a BM with the necessary mechanical properties to properly shape a tissue. Part of the egg chamber's appeal has been the ostensible simplicity of the BM's role in morphogenesis. The prevailing model posits that the follicle cells build a symmetric stiffness gradient in the BM that helps to preferentially channel tissue growth along the egg chamber's AP axis [17–19,23]. However, this study has revealed unexpected complexity in the relationship between BM architecture, BM mechanics, and tissue shape that challenge us to think more deeply about this model.

We started this study with a simple hypothesis – that a mild defect in the architecture and mechanical properties of the BM in *Sema5c* egg chambers leads to mild rounding of the egg. We then generated five pieces of evidence that support this hypothesis. We showed that: (1) loss of Sema5c reduces BM fibril content and length without a concomitant defect in late-stage stress fiber alignment; (2) lowering Col IV levels, which may also lower the fibril content, dominantly enhances the egg shape defect; and (3) restoring BM fibrils to wild-type levels suppresses the egg shape defect. We next used swelling assays to compare the mechanical properties of the BMs of *Sema5c* egg chambers to those of *fat2* egg chambers to ask if this could account for the differences in egg shape between the two conditions (mildly round vs. spherical) and found that: (4) the BMs of *Sema5c* egg chambers are less resistant to rupturing than wild-type egg chambers but more resistant than those of *fat2* egg chambers, and (5) the mechanical defect in the BMs of *Sema5c* egg chambers appears later in development than those of *fat2* egg chambers, only becoming observable shortly before the elongation defect. The surprise came when we then examined the BMs of $Lar^{-/+}$ *Sema5c* egg chambers. Here, egg shape is comparable to wild type, and yet fibril content is reduced even further and the BM ruptures even more quickly in a swelling assay than when *Sema5c* alone is lost. How do we explain these perplexing results? We consider four non-mutually exclusive possibilities below.

The first possible explanation is that BM fibrils act alongside other architectural features of the BM to influence egg chamber elongation. We and others have long focused on the fibrils because it is straightforward to measure their size and density, and both can be augmented by modulating the pattern of BM secretion [21,26,40,44,46]. It is also well established that fibrils contribute to the overall stiffness of the BM and that a mild increase in BM fibril content can hyper-elongate the egg [17,21,24,25]. However, there are also more subtle polarized features in the matrix that we have previously called ridges [21]. These structures appear to form via a different mechanism than the fibrils and could act redundantly with them. If BM ridges are increased in the BMs of $Lar^{-/+}$ *Sema5c* egg chambers, it could explain why the eggs are longer than when *Sema5c* alone is lost, even though fibrils are further reduced. Redundancy between fibrils and ridges could also explain two other genetic conditions in which egg shape is normal despite BM fibrils being reduced [25,38]. Testing this hypothesis will require a better understanding of how these more subtle architectural features form, as well as new methods to measure and manipulate them.

The second possible explanation is that the osmotic swelling assay commonly used by the field does not measure the key mechanical properties of the follicular BM that are important for its role in creating the final shape of the egg. Because the follicular BM promotes elongation by providing anisotropic resistance to tissue growth, a major advantage of this assay is that it applies similar stresses to the BM as those caused by growth. However, the stresses that are applied are artificially high. Further, the way a material responds to stress often depends on the time scale over which the stress is applied. Given that egg chamber growth occurs over hours-to-days and the swelling occurs over minutes, results from this assay could be misleading. This issue is magnified when the material is an ECM, because the cells can also actively remodel the composition and/or structure of the network over that longer time frame. Indeed, when we tracked the relative change in aspect ratios over time for stage 10 egg chamber under acute swelling, the *Sema5c* condition was comparable to controls, despite the fact that *Sema5c* egg chambers will go on to make mildly round eggs (Fig. S3E). There are similar issues with the common use of atomic force microscopy (AFM) to measure BM stiffness, as this technique measures resistance to deformation perpendicular to the plane of the BM, whereas the biologically relevant deformation of the egg chamber BM would be predicted to be in plane. Stiffness is also only one of many mechanical properties of the BM network that are likely to be important for its morphogenetic function, making these values difficult to interpret in isolation.

The third possible explanation is that the way the follicular BM influences egg chamber elongation is different at later stages of egg chamber development than at earlier stages. To date, most studies of the follicular BM have focused on stage 8. This is when the stiffness gradient in the BM is at its peak, as it is just before the point that Col IV synthesis and fibril formation both cease [17,19,42]. One key feature of the *Sema5c* phenotype is that neither the elongation defect nor the mechanical defect in the BM that we measured is observable at this stage. Thus, to gain a full understanding of how the BM influences egg shape also requires examination of later stages. Notably, three studies that performed AFM on the BM at later stages all showed that the stiffness pattern changes over time, shifting from the symmetrical stiffness gradient at stage 8, to a pattern in which the BM is softer in the anterior and stiffer in the posterior at stage 10 [17,24,48]. Determining how this change in the mechanical patterning of the BM influences tissue elongation and whether this change can account for the unexpected results obtained with the $Lar^{-/+}$ *Sema5c* condition will be key areas for future research.

Finally, the fourth possible explanation is that removing one copy of *Lar* in *Sema5c* females promotes egg chamber elongation in a way that bypasses the normal requirement for the BM in this process. At early developmental stages, the BM promotes egg chamber elongation by directing polarized cell behaviors within the follicular epithelium like cell intercalation and cell lengthening [37,49]. *Sema5c* BMs are clearly sufficient to support these behaviors, as the egg chambers do not become rounder than controls until stage 12, a pattern that is also seen in some other conditions that alter BM architecture [21,26]. Notably, the nurse cells rapidly transfer their cytoplasmic contents to the oocyte during stage 11 [50]. This process may put particularly high stresses on the BM; *Sema5c* egg chambers might become rounder than controls at stage 12 because their weakened BMs fail under this additional stress. Under this model, removing one copy of *Lar* in *Sema5c* females could alter the dynamics of the cytoplasmic transfer in a way that compensates for the weakened BM in this background. However, more work is needed to understand the relationship between cytoplasmic transfer, BM mechanics, and the final stages of egg chamber elongation.

In conclusion, the results presented here make a strong case that BM fibrils directly contribute to the mechanical properties of the BM that are important for its role in egg chamber elongation. However, they also call for new ways of thinking about the BM's role in this process, as well as new methods to study it, for real understanding to emerge.

Methods

Reagents and resources

A full list of the reagents, *Drosophila* lines, and software used in this study can be found in **Table S1**.

Drosophila care

Drosophila melanogaster were reared on cornmeal molasses agar food at 25 °C using standard techniques. The genotypes used in each

experiment are listed in **Table S2**, indexed by figure panel. Females were aged on yeast with males prior to dissection; temperatures and yeasting conditions used for each experiment are in **Table S3**, indexed by figure panel.

Egg chamber dissections

Ovaries were removed from yeasted females using 1 set of Dumont #55 forceps and 1 set of Dumont #5 forceps. All dissections were performed in a spot plate with 500 μL live imaging media (Schneider's *Drosophila* medium, 1X Penicillin-Streptomycin, 15 % fetal bovine serum, and 200 μg/mL insulin) [51] except for those used to determine egg aspect ratios or in osmotic swelling assays, as described below. Ovarioles were mechanically removed from the muscle sheath with forceps. For additional methods and videos of dissection, see Cetera et al. [52]

Fixation and F-actin staining

Following dissection in live imaging media, ovarioles were fixed for 15 min in 4 % EM grade formaldehyde in PBT (phosphate buffered saline + 0.1 % Triton X-100) and then washed 3 × 5 min in PBT. If TRITC-phalloidin was used, it was added at a concentration of 1:300 during the fixation step. If AlexaFluor™ 647-phalloidin was used, egg chambers were stained after washing at a concentration of either 1:30 in PBT for 2–4 hr at room temperature or 1:50 in PBT overnight at 4 °C; egg chambers were then washed 3 × 5 min in PBT. DAPI was added at a concentration of 1:600 concurrent with phalloidin staining. Ovarioles were mounted in ~35 μL of SlowFade Diamond antifade on a slide using a 22×50 mm #1.5 coverslip, sealed with nail polish, and stored at 4 °C until imaged. For more details, see Anderson et al. [53]

Dissection and fixation for mature egg aspect ratio measurements

Ovarioles were dissected in freshly made Robb's minimal saline and fixed in Robb's containing 8 % EM grade formaldehyde for 5 min. The tissue was washed 3 × 5 min in PBT, then disrupted with pipetting to remove the muscle sheath. Tissue was stained with TRITC-phalloidin (1:300) and DAPI (1:600) for 15 min. Ovarioles were then washed 3 × 5 min in PBT and mounted in ~35 μL of SlowFade Diamond antifade on a slide using a 22×50 mm #1.5 coverslip, sealed with nail polish, and stored at 4 °C until imaged.

Live imaging sample preparation

For live imaging, ovarioles were dissected in live imaging media and quickly moved to a fresh well of live imaging media in a spot plate, containing CellMask Orange at a dilution of 1:500. Egg chambers were incubated with CellMask for 10–15 min. Ovarioles were then washed in fresh live imaging media to remove excess stain. To prepare a slide for live imaging, 1–5 ovarioles were transferred in 20 μL of live imaging media to a clean glass slide. 48–51 μm diameter glass beads were added to support a 22×22 mm #1.5 coverslip and limit egg chamber compression. Coverslip edges were sealed with melted petroleum jelly to limit evaporation during imaging. Samples were checked for damage using CellMask and excluded if damage was observed. Slides were used for no >1 hr.

Osmotic swelling assay

The osmotic swelling assay was adapted from previous studies, [17, 39], with a few key differences. Egg chambers were dissected into 500 μL Adult Hemolymph-Like Saline (AHLS) [54] rather than live imaging media. Ovarioles were trimmed by cutting through the stalk with a 27-guage needle to remove egg chambers older than the stage of interest The dissecting media was exchanged 2x with either 0.01X AHLS (stage 8) or 0.2X AHLS (stage 8 and 10), and then the egg chambers were transferred to a 35 mm x 10 mm polystyrene culture dish containing 2 mL of the same concentration of diluted AHLS. Egg chambers were neither adhered to the dish, nor were they coverslipped to avoid additional exogenous stresses during the procedure.

Latrunculin and collagenase treatment

Egg chambers were dissected in live imaging media as described above. Latrunculin A (50 μM in dimethyl sulfoxide (DMSO), Enzo Life Sciences) or collagenase (1000 U/mL CLSPA in Schneider's *Drosophila* medium and 1X Penicillin-Streptomycin; Worthington Biochemical Corp.) were added to a final volume of 100 μL of live imaging media. DMSO (1 %) was used as a control. For latrunculin A experiments, egg chambers were incubated at 29 °C for 4 hours, protected from light. For collagenase experiments, egg chambers were incubated at room temperature for 2 hours, protected from light. Egg chambers were then fixed, stained with 647-phallodin and DAPI, and mounted as described above. The presence of nuclei visualized with DAPI was used to confirm the loss of stress fibers due to disassembly and not to damage of the follicle cells in the latrunculin A experiments.

Fixed and live laser scanning confocal imaging

Imaging was performed on a Zeiss LSM 800 laser scanning confocal microscope run by Zen 2.3 Blue acquisition software (Zeiss) with a 10x/0.3 NA EC Plan-NEOFLUAR objective or a 40x /1.3 NA EC Plan-NEOFLUAR oil immersion objective, diode lasers (405, 488, 561, and 640 nm), and GaAsP detectors. Imaging was performed at room temperature. Used in Figures 1D-J, 2A-G, 3A-C, 4A-E, 5A-E, S1A-D and S3A-D.

Brightfield imaging

Imaging was performed on a Leica M125 stereomicroscope with a 1.0x Plan APO objective. Images were captured with a personal computer running Point Grey FlyCap2 software (Teledyne) and attached to a Grasshopper3 GS3-U3–41C6NIR camera (Teledyne). Used in Figs. 3E-H, 4F-G, S2A-C and S3E.

Measurement of BM fibril fraction and Col IV-GFP and Trol-GFP mean intensity

BM fibril fraction and BM mean intensity were measured as previously described [21]. Briefly, a confocal section capturing the entire thickness of the BM (labelled with Col IV-GFP or Trol-GFP) of a stage 8 egg chamber was acquired. All images were obtained at the same settings. Because the BM typically did not take up the entire image, the largest representative rectangle was cropped to remove non-BM pixels. The mean intensity of all pixels was measured to determine overall BM intensity. To isolate fibrils in each micrograph, an intensity threshold of 1.35x the median image intensity was applied independently and then an object size threshold of 20 pixels was applied to remove image noise. The fibril fraction was measured by dividing the sum intensity of all pixels in the isolated 'fibrils' by the sum intensity of all pixels in the image.

Measurement of BM fibril length

BM fibrils were isolated computationally as described above. An ellipse was fit for each BM fibril using the Measure function in Fiji [55]. For each egg chamber, the ten longest fibrils were determined by taking the ten fit ellipses with the longest major axes. Ellipses were visually inspected to ensure good fit for their corresponding BM fibril; those without good fit were excluded from the analysis.

Measurement of aspect ratio

A confocal section capturing the sagittal cross section of each egg chamber or mature egg was obtained. The length of the anteroposterior (AP) axis was divided by the width of the egg chamber (perpendicular to the AP axis). For stage 12 or older egg chambers, the length and width of the oocyte only was measured. Aspect ratios closer to 1 indicate a more spherical egg chamber, whereas higher aspect ratios indicate a more elongated egg chamber.

Measurement of global stress fiber alignment

A confocal section capturing the basal stress fibers visualized with phalloidin of stage 13 egg chambers was obtained. The orientation of stress fibers in an individual cell was determined by using the Measure function of the Orientation J plugin for Fiji (ImageJ) [55,56] after manually selecting a freehand region of interest at the basal surface of each cell, excluding cell boundaries. To determine the tissue-level stress fiber alignment (order parameter) for a given egg chamber, the orientation of the stress fibers in each cell was compared to all neighboring cells using a custom Python script as previously described [20].

Measurement of follicle cell migration rates

25 min timelapse movies were acquired from egg chambers labeled with CellMask. Single confocal slices near the basal surface were captured every 30 s. A kymograph was generated from each timelapse image stack in Fiji [55] by drawing a line in the direction of migration across the width of the egg chamber. The migration rate was determined by measuring the slope of 3 lines on the kymograph corresponding to cell leading edges and averaging the values. For a detailed illustration, see Barlan et al. [34]

Measurement of BM rupturing

45 min timelapse movies were acquired of egg chambers in diluted AHLS. Single frames were captured every 30 s. Egg chambers were visually inspected for leakage of internal contents outside of the BM, indicative of BM rupture, and the time and site of rupturing were recorded. The site of rupture was recorded as the relative position along the anteroposterior axis with 0 being at the anterior pole and 1 being the posterior pole.

Estimation of egg volume

An optical sagittal section through each egg was obtained with a confocal microscope. The length and width of egg was measured from this section. Egg volume was estimated by treating each egg as a prolate spheroid, with length serving as the semi-major axis and width as the semi-minor axis.

Measurement of egg chamber aspect ratio during osmotic swelling

For stage 10 egg chambers in 0.2X (AHLS), single egg chambers were thresholded in Fiji [55], and a mask of the egg chamber for each frame of the movie was created. For each frame, the aspect ratio and area of the egg chamber was estimated by fitting an ellipse using the Measure tool. The ellipses were visually inspected to ensure good fit to the egg chamber. Egg chambers that could not be used to generate a reasonably fitted ellipse were excluded from this analysis. The aspect ratio for each egg chamber over time was normalized to its initial aspect ratio, such that the initial aspect ratio had a value of 1. For egg chambers that experienced a BM rupture, only the frames before the rupture event were considered. For egg chambers that did not experience a BM rupture, the frame of maximum area was determined, and only the frames before the egg chamber reached its maximum area were considered.

Quantification and statistical analysis

Egg chambers with visible damage from dissection or dying cells were excluded. All experiments were replicated at least once. All statistical tests were performed in Prism10. The number of biological replicates (n), specific statistical test performed, and significance for each experiment can be found in the figure legends.

Funding

This work was supported by the National Institutes of Health T32 GM007183 to MTA, and R01 GM136961 and R35 GM148485 to SH-B.

Competing interests

The authors decare no competing interests.

Acknowledements

We thank Christian Dahmann, the Bloomington *Drosophila* Stock Center, and the Kyoto Stock Center for fly lines, and members of the Horne-Badovinac lab for helpful comments on the manuscript.

Supplementary materials

Supplementary material associated with this article can be found, in the online version, at doi:10.1016/j.matbio.2025.06.001.

Data availability

Data will be made available on request.

References

[1] R. Jayadev, D.R. Sherwood, Basement membranes, Curr. Biol. 27 (2017) R207–R211, https://doi.org/10.1016/j.cub.2017.02.006.
[2] A. Pozzi, P.D. Yurchenco, R.V. Iozzo, The nature and biology of basement membranes, Matrix Biol. 57–58 (2017) 1–11, https://doi.org/10.1016/j.matbio.2016.12.009.
[3] R. Jayadev, M.R.P.T. Morais, J.M. Ellingford, S. Srinivasan, R.W. Naylor, C. Lawless, A.S. Li, J.F. Ingham, E. Hastie, Q. Chi, M. Fresquet, N.-M. Koudis, H. B. Thomas, R.T. O'Keefe, E. Williams, A. Adamson, H.M. Stuart, S. Banka, D. Smedley, Genomics England Research Consortium, D.R. Sherwood, R. Lennon, A basement membrane discovery pipeline uncovers network complexity, regulators, and human disease associations, Sci. Adv. 8 (2022) eabn2265, https://doi.org/10.1126/sciadv.abn2265.
[4] J.C. Pastor-Pareja, Atypical basement membranes and basement membrane diversity – what is normal anyway? J. Cell Sci. 133 (2020) jcs241794 https://doi.org/10.1242/jcs.241794.
[5] M.J. Randles, M.J. Humphries, R. Lennon, Proteomic definitions of basement membrane composition in health and disease, Matrix Biol. 57–58 (2017) 12–28, https://doi.org/10.1016/j.matbio.2016.08.006.
[6] W.P. Daley, K.M. Yamada, ECM-modulated cellular dynamics as a driving force for tissue morphogenesis, Curr. Opin. Genet. Dev. 23 (2013) 408–414, https://doi.org/10.1016/j.gde.2013.05.005.
[7] M.-D.-C. Díaz-de-la-Loza, B.M. Stramer, The extracellular matrix in tissue morphogenesis: No longer a backseat driver, Cells Dev. 177 (2024) 203883, https://doi.org/10.1016/j.cdev.2023.203883.
[8] M.A. Morrissey, D.R. Sherwood, An active role for basement membrane assembly and modification in tissue sculpting, J. Cell Sci. 128 (2015) 1661–1668, https://doi.org/10.1242/jcs.168021.
[9] W. Ramos-Lewis, A. Page-McCaw, Basement membrane mechanics shape development: Lessons from the fly, Matrix Biol. 75–76 (2019) 72–81, https://doi.org/10.1016/j.matbio.2018.04.004.
[10] D.R. Sherwood, Basement membrane remodeling guides cell migration and cell morphogenesis during development, Curr. Opin. Cell Biol. 72 (2021) 19–27, https://doi.org/10.1016/j.ceb.2021.04.003.
[11] U. Töpfer, Basement membrane dynamics and mechanics in tissue morphogenesis, Biol. Open 12 (2023) bio059980, https://doi.org/10.1242/bio.059980.
[12] S. Horne-Badovinac, D. Bilder, Mass transit: Epithelial morphogenesis in the *Drosophila* egg chamber, Dev. Dyn. 232 (2005) 559–574, https://doi.org/10.1002/dvdy.20286.
[13] A.J. Isabella, S. Horne-Badovinac, Building from the ground up: Basement membranes in *Drosophila* development, Curr. Top. Membr. 76 (2015) 305–336, https://doi.org/10.1016/bs.ctm.2015.07.001.

[14] N. Denef, Y. Chen, S.D. Weeks, G. Barcelo, T. Schüpbach, Crag regulates epithelial architecture and polarized deposition of basement membrane proteins in *Drosophila*, Dev. Cell 14 (2008) 354–364, https://doi.org/10.1016/j.devcel.2007.12.012.
[15] D.W. Lerner, D. McCoy, A.J. Isabella, A.P. Mahowald, G.F. Gerlach, T.A. Chaudhry, S. Horne-Badovinac, A Rab10-dependent mechanism for polarized basement membrane secretion during organ morphogenesis, Dev. Cell 24 (2013) 159–168, https://doi.org/10.1016/j.devcel.2012.12.005.
[16] V. Van De Bor, V. Loreau, M. Malbouyres, D. Cerezo, A. Placenti, F. Ruggiero, S. Noselli, A dynamic and mosaic basement membrane controls cell intercalation in *Drosophila* ovaries, Development 148 (2021) dev195511, https://doi.org/10.1242/dev.195511.
[17] J. Crest, A. Diz-Muñoz, D.-Y. Chen, D.A. Fletcher, D. Bilder, Organ sculpting by patterned extracellular matrix stiffness, eLife 6 (2017) e24958, https://doi.org/10.7554/eLife.24958.
[18] U. Töpfer, K.Y. Guerra Santillán, E. Fischer-Friedrich, C. Dahmann, Distinct contributions of ECM proteins to basement membrane mechanical properties in *Drosophila*, Development 149 (2022) dev200456, https://doi.org/10.1242/dev.200456.
[19] S.L. Haigo, D. Bilder, Global tissue revolutions in a morphogenetic movement controlling elongation, Science 331 (2011) 1071–1074, https://doi.org/10.1126/science.1199424.
[20] M. Cetera, G.R. Ramirez-San Juan, P.W. Oakes, L. Lewellyn, M.J. Fairchild, G. Tanentzapf, M.L. Gardel, S. Horne-Badovinac, Epithelial rotation promotes the global alignment of contractile actin bundles during *Drosophila* egg chamber elongation, Nat. Commun. 5 (2014) 5511, https://doi.org/10.1038/ncomms6511.
[21] A.J. Isabella, S. Horne-Badovinac, Rab10-Mediated secretion synergizes with tissue movement to build a polarized basement membrane architecture for organ morphogenesis, Dev. Cell 38 (2016) 47–60, https://doi.org/10.1016/j.devcel.2016.06.009.
[22] A.L. Zajac, S. Horne-Badovinac, Kinesin-directed secretion of basement membrane proteins to a subdomain of the basolateral surface in *Drosophila* epithelial cells, Curr. Biol. 32 (2022) 735–748.e10, https://doi.org/10.1016/j.cub.2021.12.025.
[23] H.O. Gutzeit, W. Eberhardt, E. Gratwohl, Laminin and basement membrane-associated microfilaments in wild-type and mutant *Drosophila* ovarian follicles, J. Cell Sci. 100 (1991) 781–788, https://doi.org/10.1242/jcs.100.4.781.
[24] J. Chlasta, P. Milani, G. Runel, J.-L. Duteyrat, L. Arias, L.-A. Lamiré, A. Boudaoud, M. Grammont, Variations in basement membrane mechanics are linked to epithelial morphogenesis, Development 144 (2017) 4350–4362, https://doi.org/10.1242/dev.152652.
[25] A. Bhatt, V. Ruffine, U. Töpfer, J. Ryu, E. Fischer-Friedrich, C. Dahmann, The WIRS motifs in Fat2 are required for *Drosophila* egg chamber rotation but not for elongation, Development 152 (2025) DEV204201, https://doi.org/10.1242/dev.204201.
[26] F.C. Campos, C. Dennis, H. Alégot, C. Fritsch, A. Isabella, P. Pouchin, O. Bardot, S. Horne-Badovinac, V. Mirouse, Oriented basement membrane fibrils provide a memory for F-actin planar polarization via the Dystrophin-Dystroglycan complex during tissue elongation, Development 147 (2020) dev186957, https://doi.org/10.1242/dev.186957.
[27] C.G. Stedden, W. Menegas, A.L. Zajac, A.M. Williams, S. Cheng, E. Özkan, S. Horne-Badovinac, Planar-polarized Semaphorin-5c and Plexin A promote the collective migration of epithelial cells in *Drosophila*, Curr. Biol. 29 (2019) 908–920.e6, https://doi.org/10.1016/j.cub.2019.01.049.
[28] A.M. Williams, S. Horne-Badovinac, Fat2 polarizes Lar and Sema5c to coordinate the motility of collectively migrating epithelial cells, J. Cell Sci. 137 (2024) jcs261173, https://doi.org/10.1242/jcs.261173.
[29] E. Theveneau, R. Mayor, Neural crest migration: interplay between chemorepellents, chemoattractants, contact inhibition, epithelial–mesenchymal transition, and collective cell migration, WIREs Dev. Biol. 1 (2012) 435–445, https://doi.org/10.1002/wdev.28.
[30] L. Tamagnone, P.M. Comoglio, To move or not to move? EMBO Rep. 5 (2004) 356–361, https://doi.org/10.1038/sj.embor.7400114.
[31] L.T. Alto, J.R. Terman, Semaphorins and their signaling mechanisms, in: J. D. Terman (Ed.), Semaphorin Signaling. Methods in Molecular Biology, Humana Press, New York, NY, 2017, pp. 1–25, https://doi.org/10.1007/978-1-4939-6448-2_1.
[32] M. Buszczak, S. Paterno, D. Lighthouse, J. Bachman, J. Planck, S. Owen, A. D. Skora, T.G. Nystul, B. Ohlstein, A. Allen, J.E. Wilhelm, T.D. Murphy, R.W. Levis, E. Matunis, N. Srivali, R.A. Hoskins, A.C. Spradling, The Carnegie Protein Trap Library: A versatile tool for D*rosophila* developmental studies, Genetics 175 (2007) 1505–1531, https://doi.org/10.1534/genetics.106.065961.
[33] A.J. Isabella, S. Horne-Badovinac, Dynamic regulation of basement membrane protein levels promotes egg chamber elongation in *Drosophila*, Dev. Biol. 406 (2015) 212–221, https://doi.org/10.1016/j.ydbio.2015.08.018.
[34] K. Barlan, M. Cetera, S. Horne-Badovinac, Fat2 and Lar define a basally localized planar signaling system controlling collective cell migration, Dev. Cell 40 (2017) 467–477.e5, https://doi.org/10.1016/j.devcel.2017.02.003.
[35] I. Viktorinová, T. König, K. Schlichting, C. Dahmann, The cadherin Fat2 is required for planar cell polarity in the *Drosophila* ovary, Development 136 (2009) 4123–4132, https://doi.org/10.1242/dev.039099.
[36] I. Viktorinová, C. Dahmann, Microtubule polarity predicts direction of egg chamber rotation in Drosophila, Curr. Biol. 23 (2013) 1472–1477, https://doi.org/10.1016/j.cub.2013.06.014.
[37] H. Alégot, P. Pouchin, O. Bardot, V. Mirouse, Jak-Stat pathway induces *Drosophila* follicle elongation by a gradient of apical contractility, eLife 7 (2018) e32943, https://doi.org/10.7554/eLife.32943.
[38] F. Aurich, C. Dahmann, A mutation in *fat2* uncouples tissue elongation from global tissue rotation, Cell Rep. 14 (2016) 2503–2510, https://doi.org/10.1016/j.celrep.2016.02.044.
[39] J.C. Pastor-Pareja, T. Xu, Shaping cells and organs in *Drosophila* by opposing roles of fat body-secreted Collagen IV and Perlecan, Dev. Cell 21 (2011) 245–256, https://doi.org/10.1016/j.devcel.2011.06.026.
[40] H.-Y. Ku, L.K. Harris, D. Bilder, Specialized cells that sense tissue mechanics to regulate *Drosophila* morphogenesis, Dev. Cell 58 (2023) 211–223.e5, https://doi.org/10.1016/j.devcel.2023.01.004.
[41] K.E. Peebles, K.S. LaFever, P.S. Page-McCaw, S. Colon, D. Wang, A.M. Stricker, N. Ferrell, G. Bhave, A. Page-McCaw, Peroxidasin is required for full viability in development and for maintenance of tissue mechanics in adults, Matrix Biol. 125 (2024) 1–11, https://doi.org/10.1016/j.matbio.2023.11.005.
[42] B. Knibiehler, C. Mirre, Y. Le Parco, Collagen type IV of *Drosophila* is stockpiled in the growing oocyte and differentially located during early stages of embryogenesis, Cell Differ. Dev. 30 (1990) 147–157, https://doi.org/10.1016/0922-3371(90)90082-8.
[43] D. Andersen, S. Horne-Badovinac, Influence of ovarian muscle contraction and oocyte growth on egg chamber elongation in *Drosophila*, Development 143 (2016) 1375–1387, https://doi.org/10.1242/dev.131276.
[44] C. Dennis, P. Pouchin, G. Richard, V. Mirouse, Basement membrane diversification relies on two competitive secretory routes defined by Rab10 and Rab8 and modulated by Dystrophin and the exocyst complex, PLoS Genet. 20 (2024) e1011169, https://doi.org/10.1371/journal.pgen.1011169.
[45] H.-Y. Ku, D. Bilder, Basement membrane patterning by spatial deployment of a secretion-regulating protease, Proc. Natl. Acad. Sci. 122 (2025) e2412161122, https://doi.org/10.1073/pnas.2412161122.
[46] U. Töpfer, J. Ryu, K.Y. Guerra Santillán, J. Schulze, E. Fischer-Friedrich, G. Tanentzapf, C. Dahmann, AdamTS proteases control basement membrane heterogeneity and organ shape in *Drosophila*, Cell Rep. 43 (2024) 114399, https://doi.org/10.1016/j.celrep.2024.114399.
[47] J. Wittes, T. Schüpbach, A. Gene, Expression screen in *Drosophila melanogaster* identifies novel JAK/STAT and EGFR targets during oogenesis, G3: Genes Genomes Genet. 9 (2018) 47–60, https://doi.org/10.1534/g3.118.200786.
[48] C. Knudsen, W.S. Koh, T. Izumikawa, E. Nakato, T. Akiyama, A. Kinoshita-Toyoda, G. Haugstad, G. Yu, H. Toyoda, H. Nakato, Chondroitin sulfate is required for follicle epithelial integrity and organ shape maintenance in *Drosophila*, Development 150 (2023) dev201717, https://doi.org/10.1242/dev.201717.
[49] D.-Y. Chen, J. Crest, S.J. Streichan, D. Bilder, Extracellular matrix stiffness cues junctional remodeling for 3D tissue elongation, Nat. Commun. 10 (2019) 3339, https://doi.org/10.1038/s41467-019-10874-x.
[50] C. Berg, M. Sieber, J. Sun, Finishing the egg, Genetics 226 (2024) iyad183, https://doi.org/10.1093/genetics/iyad183.
[51] M. Prasad, A.C.-C. Jang, M. Starz-Gaiano, M. Melani, D.J. Montell, A protocol for culturing *Drosophila melanogaster* stage 9 egg chambers for live imaging, Nat. Protoc. 2 (2007) 2467–2473, https://doi.org/10.1038/nprot.2007.363.
[52] M. Cetera, L. Lewellyn, S. Horne-Badovinac, Cultivation and live imaging of *Drosophila* ovaries, in: C. Dahmann (Ed.), Drosophila. Methods in Molecular Biology, Humana Press, New York, NY, 2016, pp. 215–226. https://doi.org/10.1007/978-1-4939-6371-3_12.
[53] M.T. Anderson, K. Sherrard, S. Horne-Badovinac, Optimized fixation and phalloidin staining of basally localized F-actin networks in collectively migrating follicle cells, in: M.S. Giedt, T.L. Tootle (Eds.), Drosophila Oogenesis. Methods in Molecular Biology, Humana, New York, NY, 2023, pp. 179–191, https://doi.org/10.1007/978-1-0716-2970-3_9.
[54] K. Singleton, R.I. Woodruff, The osmolarity of adult *Drosophila* hemolymph and its effect on oocyte-nurse cell electrical polarity, Dev. Biol. 161 (1994) 154–167, https://doi.org/10.1006/dbio.1994.1017.
[55] J. Schindelin, I. Arganda-Carreras, E. Frise, V. Kaynig, M. Longair, T. Pietzsch, S. Preibisch, C. Rueden, S. Saalfeld, B. Schmid, J.-Y. Tinevez, D.J. White, V. Hartenstein, K. Eliceiri, P. Tomancak, A. Cardona, Fiji: an open-source platform for biological-image analysis, Nat. Methods 9 (2012) 676–682, https://doi.org/10.1038/nmeth.2019.
[56] R. Rezakhaniha, A. Agianniotis, J.T.C. Schrauwen, A. Griffa, D. Sage, C.V. C. Bouten, F.N. van de Vosse, M. Unser, N. Stergiopulos, Experimental investigation of collagen waviness and orientation in the arterial adventitia using confocal laser scanning microscopy, Biomech. Model. Mechanobiol. 11 (2012) 461–473, https://doi.org/10.1007/s10237-011-0325-z.